Deformation effects on isoscalar giant resonances in ^{24}Mg

Y. K. Gupta,[*] U. Garg, J. Hoffman,[†] J. Matta,[‡] P. V. Madhusudhana Rao,[§] D. Patel,[‖] and T. Peach
Physics Department, University of Notre Dame, Notre Dame, IN 46556, USA

K. Yoshida
Graduate School of Science and Technology, Niigata University, Niigata 950-2181, Japan
and Center for Computational Sciences, University of Tsukuba, Tsukuba 305-8577, Japan

M. Itoh,[¶] M. Fujiwara, K. Hara, H. Hashimoto, K. Nakanishi, and M. Yosoi
Research Center for Nuclear Physics, Osaka University, Osaka 567-0047, Japan

H. Sakaguchi, S. Terashima, S. Kishi, T. Murakami, M. Uchida,[#] and Y. Yasuda
Department of Physics, Kyoto University, Kyoto 606-8502, Japan

H. Akimune
Department of Physics, Konan University, Hyogo 658-8501, Japan

T. Kawabata[**]
Center for Nuclear Study, University of Tokyo, Wako, Saitama 351-0198, Japan

M. N. Harakeh
KVI-CART, University of Groningen, 9747 AA Groningen, The Netherlands
(Received 21 February 2016; published 21 April 2016)

Strength distributions for isoscalar giant resonances with multipolarity $L \leqslant 2$ have been determined in ^{24}Mg from "instrumental background-free" inelastic scattering of 386-MeV α particles at extreme forward angles, including 0°. The isoscalar $E0$, $E1$, and $E2$ strengths are observed to be $57 \pm 7\%$, $111.1^{+10.9}_{-7.2}\%$, and $148.6 \pm 7.3\%$, respectively, of their energy-weighted sum rules in the excitation energy range of 6 to 35 MeV. The isoscalar giant monopole (ISGMR) and quadrupole (ISGQR) resonances exhibit a prominent K splitting which is consistent with microscopic theory for a prolate-deformed ground state of ^{24}Mg. For the ISGQR it is due to splitting of the three K components, whereas for the ISGMR it is due to its coupling to the $K = 0$ component of the ISGQR. Deformation effects on the isoscalar giant dipole resonance are less pronounced, however.

DOI: 10.1103/PhysRevC.93.044324

I. INTRODUCTION

Giant resonances (GRs) are the high-frequency collective excitations of finite nuclear systems [1]. Understanding the strength distributions of these GRs in a wide range of atomic nuclei yields valuable information about the finite nuclei as well as about the bulk nuclear matter [2,3]. The isoscalar monopole and dipole modes are the "compressional modes" and are especially important because their resonance energies are directly related to the nuclear incompressibility [4]. In this context, investigating the "compressional modes" in a wide variety of nuclei is crucial.

Giant resonances being collective excitations, their strength distributions depend strongly on the nuclear shape [2]. Splitting of the isovector giant dipole resonance (IVGDR) strength due to ground-state deformation is a well established effect, attributed to different frequencies of oscillation along the major and minor axes [5]. Deformation effects on isoscalar giant monopole and giant quadrupole resonances (ISGMR and ISGQR) have been observed in some rare-earth nuclei [6–9] and in fission decay of ^{238}U [10]. These are understood in terms of K splitting: microscopic calculations based on the quasiparticle random-phase approximation (QRPA) [11], for example, predict K splitting of the multipole strength even in light deformed nuclei such as ^{24}Mg [12,13].

Identification of full giant-resonance strengths in the lighter-mass nuclei ($A < 60$) has generally been a challenge

[*]Permanent address: Nuclear Physics Division, Bhabha Atomic Research Centre, Mumbai 400 085, India.
[†]Present address: Volcano Corporation, San Diego, CA 92130, USA.
[‡]Present address: Physics Division, Oak Ridge National Laboratory, Oak Ridge, TN 37380, USA.
[§]Present address: Department of Nuclear Physics, Andhra University, Visakhapatnam 530 030, India.
[‖]Present address: M.D. Anderson Cancer Center, Houston, TX 77030, USA.
[¶]Present address: Cyclotron and Radioisotope Center, Tohoku University, Sendai 980-8578, Japan.
[#]Present address: Department of Physics, Tokyo Institute of Technology, Tokyo 152-8850, Japan.
[**]Present address: Department of Physics, Kyoto University, Kyoto 606-8502, Japan.

due to fragmentation of the strength [14–22], significant overlap of giant resonance strengths for $L \leqslant 2$, uncertainties in the extraction of the strength distributions, and overlap of the multipole strength with other direct processes (knock-out and quasifree processes, for example). The light nuclei, in particular the deformed ones such as ^{24}Mg and ^{28}Si, provide a vital testing ground for the aforementioned QRPA and deformed Hartree-Fock-Bogoliubov (HFB) calculations [12,13].

Recently, we reported evidence for the splitting of ISGMR strength in ^{24}Mg. This was the first time that such a splitting had been observed in a light-mass nucleus, indeed in any nucleus other than the well-deformed Sm nuclei and ^{238}U [23]. Owing to directional symmetry, monopole strength cannot split itself, but the observed "splitting" results from the mixing of ISGMR and the $K = 0$ component of the ISGQR. The ISGQR and the isoscalar giant dipole resonance (ISGDR), on the other hand, increase in width due to the K splitting and, for the ISGDR, also to mixing with the high-energy octupole resonance (HEOR) [7,24]. While HFB+QRPA calculations [11] are, in general, consistent with the experimental data for deformed nuclei in the rare-earth region, previous measurements on ^{24}Mg [25–28], had not shown any discernible K splitting.

In this paper, we report ISGMR, ISGDR, and ISGQR strength distributions in the prolate-deformed light-mass nucleus ^{24}Mg, as obtained from "instrumental background free" 386-MeV inelastic α scattering at extreme forward angles, including 0°. A consistent picture emerges of K splitting in ISGMR and ISGQR strength distributions due to ground-state deformation; the effect of ground-state deformation on ISGDR is, however, less pronounced.

II. EXPERIMENTAL PROCEDURES

Inelastic scattering of 386-MeV α particles was measured at the Ring Cyclotron Facility of the Research Center for Nuclear Physics (RCNP), Osaka University. A self-supporting foil (0.7 mg/cm^2) of enriched (>99%) ^{24}Mg was employed as the target. Inelastically scattered α particles were momentum analyzed with the high-resolution magnetic spectrometer "Grand Raiden" [29]. The horizontal and vertical positions of the α particles were measured using the focal-plane detector system composed of two position-sensitive multiwire drift chambers (MWDCs) and two plastic scintillators [7].

Data for elastic scattering and inelastic scattering to the low-lying states were taken in the angular range of 3.5° to 26.5°. Giant-resonance measurements were performed at the very forward angles of the spectrometer (from 0° to 10.4°). Using the ray-tracing technique, the angular width of 1.8° for each central angle was divided into five equal regions during ofline data analysis. The angular resolution of the MWDCs, including the nominal broadening of scattering angle due to the emittance of the ^{4}He^{2+} beam and the multiple Coulomb-scattering effects, was about 0.15°.

Measurements were made for two magnetic-field settings of the Grand Raiden spectrometer, resulting in spectra covering excitation energies of about 4 to 27 MeV and 24 to 50 MeV (the low-E_x and the high-E_x spectra, respectively). Data were also taken with a ^{12}C target at each setting of the angle and magnetic field of the spectrometer, providing precise energy calibrations. Energy losses of the incident beam and outgoing α particles were taken into account in creating the final excitation-energy spectra. The high-E_x spectrum connects smoothly, and without any normalization, with the low-E_x spectrum, as discussed in Ref. [23].

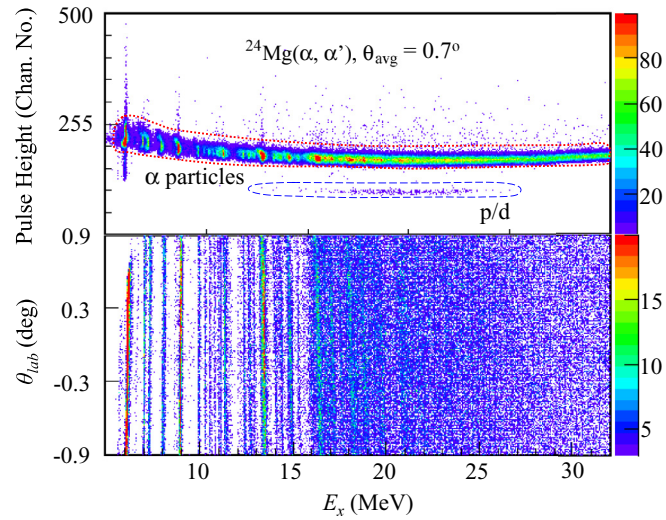

FIG. 1. Top panel: A two-dimensional scatter plot of pulse height from the first plastic scintillator detector versus excitation energy (E_x) at an averaged angle, $\theta_{avg} = 0.7°$. Bottom panel: A two-dimensional scatter plot of θ_{lab} versus E_x (see text).

The MWDCs and scintillators enabled us to make particle identification and to reconstruct the trajectories of scattered particles. Figure 1(a) shows a typical particle identification plot at an averaged angle, $\theta_{avg} = 0.7°$. The α particles are

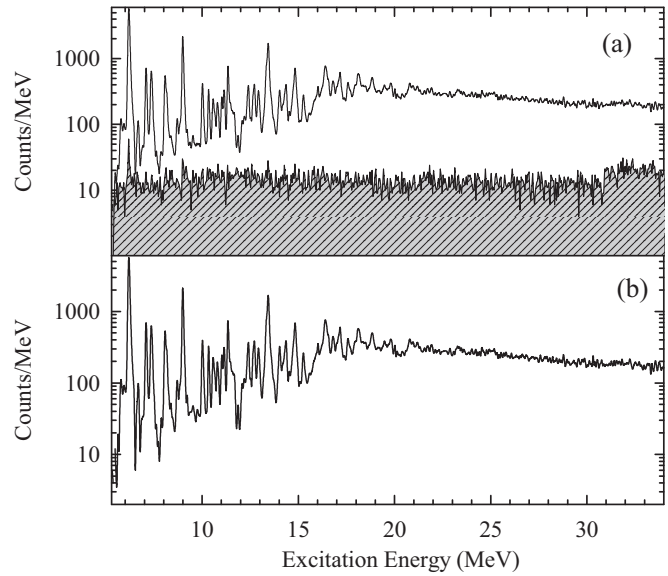

FIG. 2. (a) Excitation-energy spectrum at an averaged spectrometer angle, $\theta_{avg} = 0.7°$ before subtracting the instrumental background (gray hatched region). (b) Excitation-energy spectrum after subtracting the instrumental background.

observed to be well separated from other particles arriving at the focal plane. Figure 1(b) shows a typical two-dimensional scatter plot of the scattering angle, $\theta_{\rm lab}$, versus the excitation energy, E_x. Different discrete states of ^{24}Mg are clearly visible below $E_x = 20$ MeV. The excitation energies of these discrete states overlapped very well at different spectrometer angles in the range of 0° to 10.4°, establishing precise energy calibration. Impurities of ^{1}H, ^{12}C, and ^{16}O in the target were identified with the help of kinematics. Scattering events from these impurity nuclei were observed to be clearly separated from ^{24}Mg except for a few energy and angular bins.

The vertical-position spectrum obtained in the double-focusing mode of the spectrometer was exploited to eliminate the instrumental background [7,30]. Figure 2(a) shows typical instrumental background (gray-hatched region) and excitation-energy spectrum before the background subtraction at an averaged spectrometer angle of $\theta_{\rm avg} = 0.7^\circ$. The excitation-energy spectrum after subtracting this instrumental background is depicted in Fig. 2(b). The instrumental background is almost constant over the entire excitation-energy spectrum and constitutes a maximum of around 20% of the total spectrum at spectrometer position of 0°, decreasing rapidly with increasing angles.

III. DATA ANALYSIS

The excitation spectra for inelastic-scattering cross sections were divided into energy bins of different sizes. For E_x from 4 to 20 MeV, the size of the energy bin was chosen to accommodate the discrete peaks. Because the discrete structure of the strength distribution diminishes for $E_x > 21$ MeV (see Fig. 2), the bin size in this energy domain was chosen to be 1 MeV to reduce statistical fluctuations. The laboratory angular distribution for each excitation-energy bin was converted to the center-of-mass frame using the standard Jacobian and relativistic kinematics. Typical angular distributions are shown in Fig. 3. The experimental angular distributions thus obtained consist of contributions from various multipoles; a multipole-decomposition analysis (MDA) was, therefore, carried out to extract the ISGMR, ISGDR, and ISGQR strengths. In the MDA

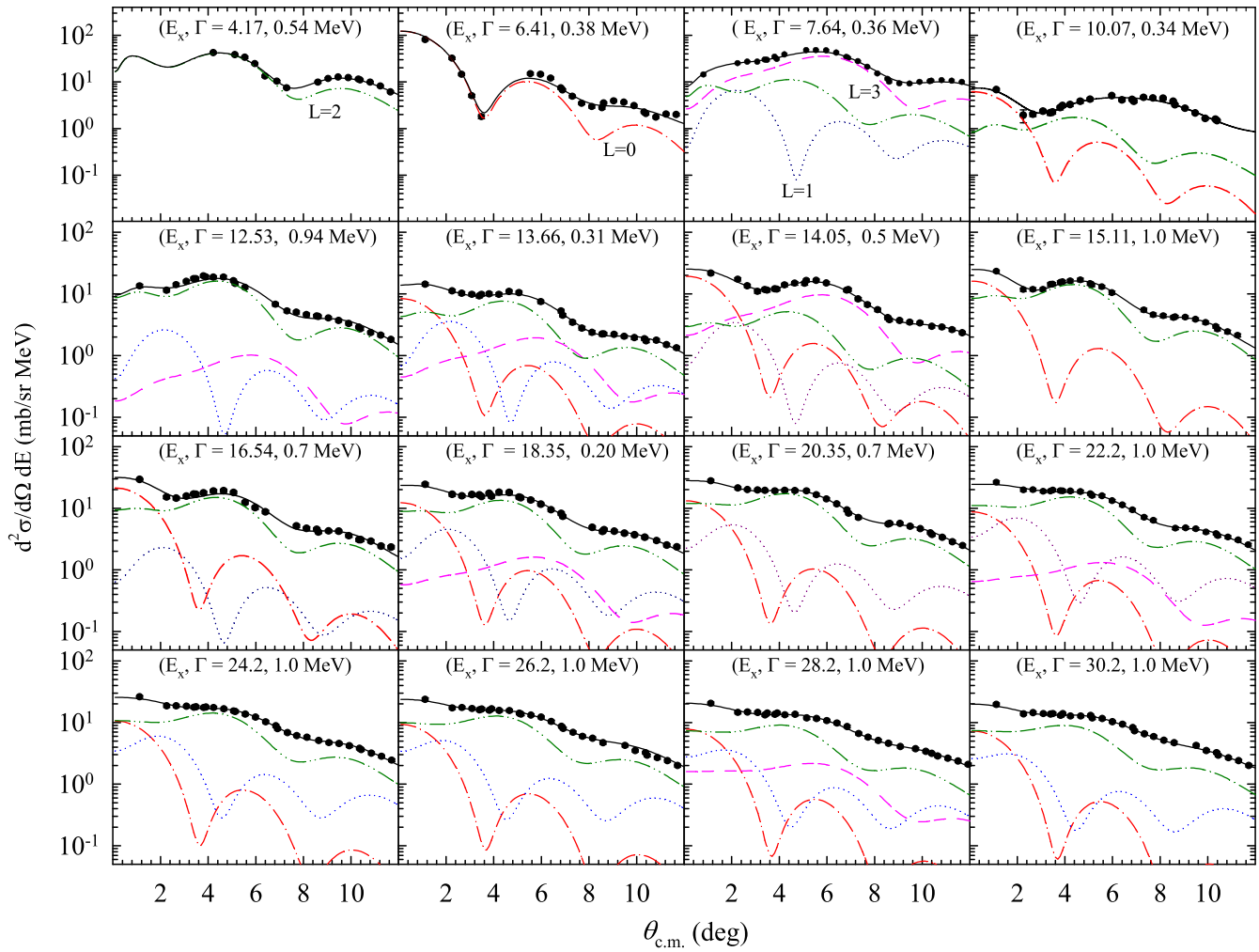

FIG. 3. Typical angular distributions of inelastic α scattering from ^{24}Mg. The solid line (black) through the data shows the sum of various multipole components obtained from MDA. The dash-dotted (red), dotted (blue), dash-double-dotted (green), and dashed (pink) curves show contributions from $L = 0$, 1, 2, and 3, respectively, with the transferred angular momentum L specified along with the curves. The mean E_x value as well as the bin width Γ are also shown for each case.

process, the experimental double-differential cross sections are expressed as linear combinations of calculated DWBA double-differential cross sections for different multipoles as

$$\frac{d^2\sigma^{\exp}(\theta_{\text{c.m.}},E_x)}{d\Omega dE} = \sum_{L=0}^{6} a_L(E_x)\frac{d^2\sigma_L^{\text{DWBA}}(\theta_{\text{c.m.}},E_x)}{d\Omega\, dE} \qquad (1)$$

where $a_L(E_x)$ is EWSR fraction for the Lth multipole, and $\frac{d^2\sigma_L^{\text{DWBA}}}{d\Omega\, dE}(\theta_{\text{c.m.}},E_x)$ is the calculated DWBA cross section corresponding to 100% EWSR for the Lth multipole. The $a_L(E_x)$ are determined using the χ^2 minimization technique, with the uncertainties estimated by changing the magnitude of the one component $a_L(E_x)$, until refitting by varying the other components resulted in an increase in the χ^2 by 1 [7,25,27].

The DWBA calculations were performed employing the "hybrid" optical-model potential (OMP) proposed by Satchler and Khoa [31]. In this procedure, the real part of the OMP is generated by single folding with a density-dependent Gaussian α-nucleon interaction [32]. A Woods-Saxon potential is used for the imaginary term of the OMP. Therefore, the total α-nucleus ground-state potential is given by

$$U(r) = -V(r) - iW/\{1 + \exp[(r - R_I)/a_I]\}, \qquad (2)$$

where $V(r)$ is the real single-folding potential obtained using the computer code SDOLFIN by folding the ground-state density with the density-dependent α-nucleon interaction. W is the depth of the Woods-Saxon type imaginary part of the potential, with the radius R_I and diffuseness a_I. The imaginary potential parameters (W, R_I, and a_I), together with the depth of the real part, V, are obtained by fitting the elastic-scattering cross sections using the computer code PTOLEMY [33,34]. The best fit to the elastic cross-section data (normalized to the Rutherford cross section) obtained from minimization of χ^2 is shown in Fig. 4(a). The OMP parameters thus determined are presented in Table I.

The angular distribution for the 1.368-MeV 2^+ state in ^{24}Mg was calculated in the distorted-wave Born approximation (DWBA) framework using the known $B(E2)$ value from the literature (also provided in Table I) and the OMP parameters thus obtained. An excellent agreement between the calculated and experimental angular distributions for the 2^+ state, as shown in Fig. 4(b), establishes the appropriateness of the OMP parameters. The collective isoscalar transition densities were taken from Refs. [2,36,37]. Radial moments for ^{24}Mg were obtained by numerical integration of the Fermi mass distribution assuming the mean charge radius $c = 3.0453$ fm and diffuseness $a = 0.523$ fm [38]. Using the transition densities, the real term of the transition potential was obtained using the computer code DOLFIN [39], whereas the imaginary term of the transition potential was obtained from analytical differentiation of the Woods-Saxon potential multiplied by the corresponding deformation length. DWBA cross sections for each excitation energy (E_x) were obtained for natural parities of the multipolarities from $L = 0$–6. EWSR fractions for each multipolarity (a_L) are determined using the MDA technique. Results of MDA fits to angular distribution data for typical energy bins are shown in Fig. 3 along with the contributions from the $L = 0$, 1, 2, and 3 multipoles. The strength distributions are obtained from the experimentally

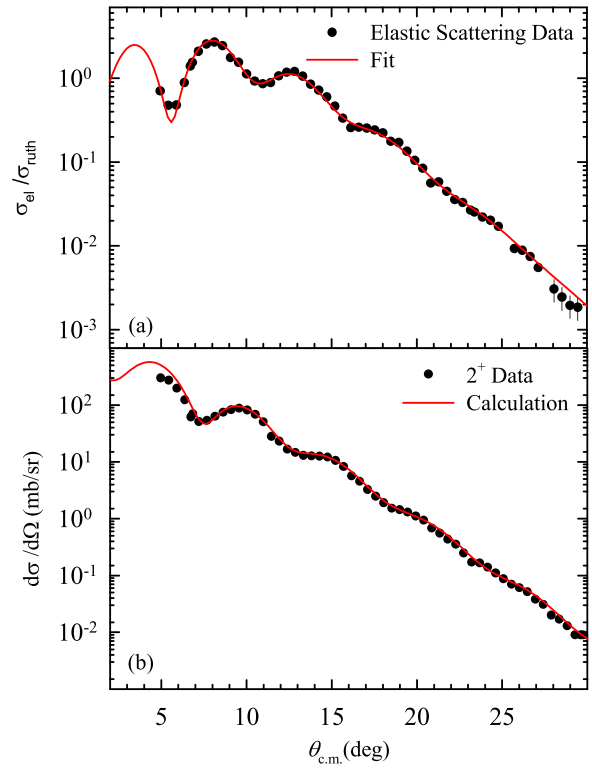

FIG. 4. (a) Angular distribution of the ratio of the differential cross sections for elastic scattering to Rutherford scattering for 386-MeV α particles from ^{24}Mg. The solid red line is the result of a "hybrid" optical-model fit to the data. (b) Angular distribution of differential cross sections for the 1.368 MeV 2^+ state in ^{24}Mg. The solid red line shows the result of the DWBA calculation (see text).

determined EWSR fraction (a_L) using the relations provided in Ref. [2]. Following this procedure, $B(EL)$ values were determined for several discrete states in ^{24}Mg and compared with the values reported in the literature, as discussed in Ref. [23]. A close agreement with the previous results for most of the cases further established the reliability of optical model parameters and the MDA procedure.

The experimentally determined ISGMR strength distribution in ^{24}Mg is shown in Fig. 5. The distribution consists of a clear two-peak structure: a narrow peak at $E_x \sim 16$ MeV and a broad peak at $E_x \sim 24$ MeV. A total of $57 \pm 7\%$ $E0$ EWSR is exhausted over the excitation-energy region of 6 to 35 MeV. The two-peak structure is in contrast with the broad ISGMR distributions reported in previous works [25,26] and is, in fact, very similar to the ISGMR distribution observed in ^{154}Sm [8], thus strongly indicative of one resulting from the deformation

TABLE I. Optical-model parameters obtained by fitting the elastic-scattering data. Also listed is the $B(E2)$ value for the 1.368-MeV 2^+ state in ^{24}Mg from Ref. [35].

V (MeV)	W (MeV)	R_I (fm)	a_I (fm)	R_C (fm)	$B(E2)$ (e^2b^2)
33.1	36.1	3.87	0.778	3.04	0.0432

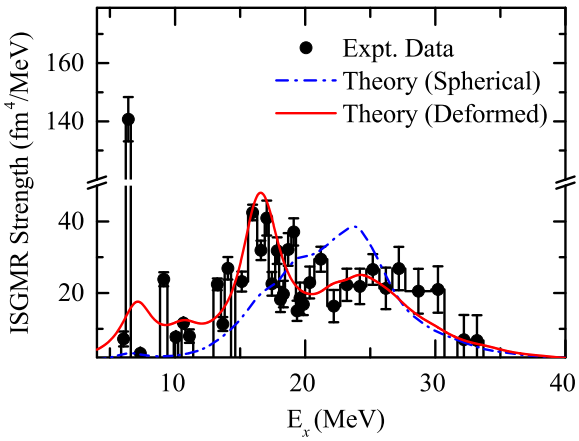

FIG. 5. ISGMR strength distributions in ^{24}Mg. The dash-dotted (blue) and solid (red) lines show microscopic calculations for spherical and prolate ground-state deformation, respectively.

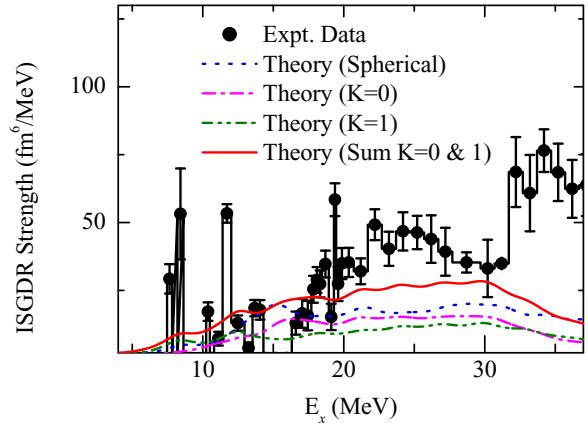

FIG. 6. ISGDR strength distributions in ^{24}Mg. The dotted (blue) line shows microscopic calculations for the spherical ground state. The dash-dotted (magenta), dash-double-dotted (green), and solid (red) lines show microscopic calculations for prolate ground-state deformation for $K = 0,1$ and the sum of $K = 0$ and 1, respectively.

of the ground state. A comparison of the experimental and theoretical strength distributions further establishes that this structure corresponds to that of a deformed nucleus.

The theoretical strength distributions were obtained as a self-consistent solution of the deformed HFB and QRPA equations employing the Skyrme SkM* functional [40]. Details of the calculation scheme can be found in Refs. [11,41]. In the present calculations, the smearing width of 3 MeV was introduced to take into account the spreading effects. The SkM* functional gives an intrinsic quadrupole moment $Q_0 = 54.0\,e\,\mathrm{fm}^2$, which is consistent with the measured $B(E2)$ of the first 2^+ state listed in Table I. In the energy region of 6 to 35 MeV, the obtained IS monopole strength exhausts 83% of EWSR. Thus, the theoretical strengths have been scaled down by a factor $0.57/0.83 \sim 0.68$ in Fig. 5 for comparison with the experimental data. This mismatch between theoretical and experimental strengths is not too worrisome considering that the experimental strengths can have ~20% systematic uncertainty resulting from the choice of the OMPs used and the DWBA calculations, as has been noted in previous works as well [2,32,42]. In addition to the strengths obtained for the prolate-deformed ground state, the strength distributions are obtained for a spherical configuration for comparison. The prominent peak around 16 MeV in the ISGMR strength distribution appears only when the ground state is deformed.

The ISGDR strength distribution in ^{24}Mg is shown in Fig. 6, and consists of a broad peak centered around 25 MeV. A total of $111.1^{+10.9}_{-7.2}$% EWSR is exhausted over the excitation-energy region of 6 to 35 MeV. Unlike the ISGMR, the deformation effects on ISGDR are not very pronounced either in the experimental data or in the theoretical strength distributions (also shown in Fig. 6). The rising strength at the highest excitation energies is, most likely, spurious, resulting from direct processes (knock-out and quasifree processes, for example) that mimic the angular distributions of ISGDR [42].

The experimentally determined ISGQR distribution in ^{24}Mg is shown in Fig. 7. In contrast with the pronounced peak observed in the heavier nuclei ($A \geqslant 90$), the ISGQR distribution for ^{24}Mg is quite broad. Microscopic calculations for ISGQR are compared with the experimental data in the Fig. 7. The theory predicts a peak close to 22 MeV, consistent with $65A^{-1/3}$ MeV for a spherical ground state. Similar to ISGMR, the prolate ground state of ^{24}Mg pushes the ISGQR peak to lower energies with significant broadening due to K splitting. Theoretical prediction of the division of the ISGQR strength into individual components, $K = 0$, 1, and 2, is also shown in Fig. 7. The sum of these components in the energy region 15–25 MeV is in reasonable agreement with the data. Again, comparison of data with the spherical and deformed ground-state microscopic calculations clearly indicates that ISGQR strength fragmentation in ^{24}Mg corresponds to a prolate-deformed ground state. A total of $148 \pm 8\%$ $E2$ EWSR is exhausted over the excitation-energy region of 6 to 35 MeV.

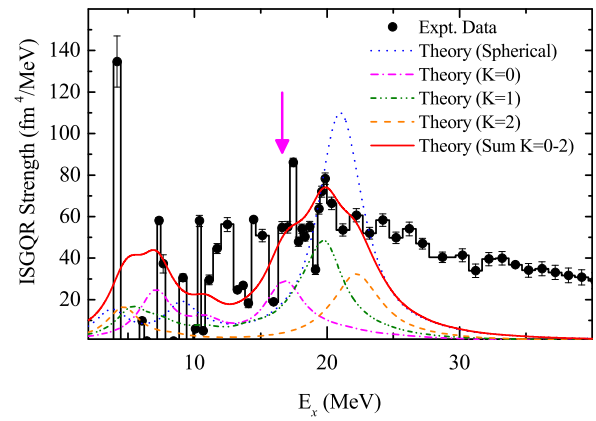

FIG. 7. ISGQR strength distributions in ^{24}Mg. The dotted (blue) line shows microscopic calculations for the spherical ground state. The dash-dotted (magenta), dash-double-dotted (green), dashed (orange), and solid (red) lines show microscopic calculations for prolate ground-state deformation for $K = 0,1,2$ and the sum of $K = 0$ to 2, respectively. The arrow indicates the peak position of $K = 0$ component.

The position of the $K = 0$ peak of ISGQR coincides with the narrow peak of the ISGMR strength distribution at around 16 MeV. This clearly shows that splitting of ISGMR strength distribution is due to mixing with the $K = 0$ component of ISGQR; otherwise, the monopole has no directional projection and therefore the ISGMR cannot itself produce the splitting of the strength.

In summary, we have measured the isoscalar giant resonance strength distributions for $L \leqslant 2$ in the light nucleus ^{24}Mg via small-angle inelastic scattering of α particles. We observe a two-peak structure in the ISGMR strength, which is attributable to coupling to the $K = 0$ component of ISGQR due to ground-state deformation. The observed strength distributions for ISGMR and ISGQR are in good agreement with microscopic calculations for a prolate-deformed ground state in ^{24}Mg, and are in contrast with those expected for a spherical ground state. This is the first time that the K splitting of the ISGMR and ISGQR has been observed in a very light nucleus. The deformation effects on ISGDR are not clearly discernible in the present data.

ACKNOWLEDGMENTS

The authors acknowledge the efforts of the staff of the RCNP Ring Cyclotron Facility in providing a high-quality, halo-free α beam required for the measurements reported in this paper, and are grateful to Prof. G. Colò for many discussions about the theoretical aspects of this work. This work has been supported in part by the US National Science Foundation (Grants No. INT-9910015, No. PHY04-57120, and No. PHY-1419765), and by the JSPS KAKENHI (Grants No. 23740223 and No. 25287065). The numerical calculations were performed on SR16000 at the Yukawa Institute for Theoretical Physics, Kyoto University.

[1] F. E. Bertrand, Nucl. Phys. A **354**, 129 (1981).
[2] M. N. Harakeh and A. van der Woude, *Giant Resonances Fundamental High-Frequency Modes of Nuclear Excitation* (Oxford University Press, New York, 2001).
[3] J. M. Lattimer and M. Prakash, Astrophys. J. **550**, 426 (2001).
[4] S. Stringari, Phys. Lett. B **108**, 232 (1982).
[5] J. M. Eisenberg and W. Greiner, *Nuclear Models*, Vol. 1 (Elsevier Science, Amsterdam, 1975).
[6] U. Garg, P. Bogucki, J. D. Bronson, Y.-W. Lui, C. M. Rozsa, and D. H. Youngblood, Phys. Rev. Lett. **45**, 1670 (1980).
[7] M. Itoh, H. Sakaguchi, M. Uchida, T. Ishikawa, T. Kawabata, T. Murakami, H. Takeda, T. Taki, S. Terashima, N. Tsukahara *et al.*, Phys. Rev. C **68**, 064602 (2003).
[8] D. H. Youngblood, Y.-W. Lui, and H. L. Clark, Phys. Rev. C **60**, 067302 (1999).
[9] D. H. Youngblood, Y.-W. Lui, H. L. Clark, B. John, Y. Tokimoto, and X. Chen, Phys. Rev. C **69**, 034315 (2004).
[10] S. Brandenburg, R. De Leo, A. G. Drentje, M. N. Harakeh, H. Janszen, and A. van der Woude, Phys. Rev. Lett. **49**, 1687 (1982).
[11] K. Yoshida and T. Nakatsukasa, Phys. Rev. C **88**, 034309 (2013).
[12] K. Yoshida, Mod. Phys. Lett. A **25**, 1783 (2010).
[13] S. Péru and H. Goutte, Phys. Rev. C **77**, 044313 (2008).
[14] F. E. Bertrand, K. van der Borg, A. G. Drentje, M. N. Harakeh, J. van der Plicht, and A. van der Woude, Phys. Rev. Lett. **40**, 635 (1978).
[15] K. van der Borg, M. N. Harakeh, and A. van der Woude, Nucl. Phys. A **365**, 243 (1981).
[16] S. Brandenburg, R. De Leo, A. G. Drentje, M. N. Harakeh, H. Sakai, and A. van der Woude, Phys. Lett. B **130**, 9 (1983).
[17] F. Zwarts, A. G. Drentje, M. N. Harakeh, and A. van der Woude, Nucl. Phys. A **439**, 117 (1985).
[18] H. J. Lu, S. Brandenburg, R. De Leo, M. N. Harakeh, T. D. Poelhekken, and A. van der Woude, Phys. Rev. C **33**, 1116 (1986).
[19] M. Itoh, S. Kishi, H. Sakaguchi, H. Akimune, M. Fujiwara, U. Garg, K. Hara, H. Hashimoto, J. Hoffman, T. Kawabata *et al.*, Phys. Rev. C **88**, 064313 (2013).
[20] Y.-W. Lui, J. D. Bronson, C. M. Rozsa, D. H. Youngblood, P. Bogucki, and U. Garg, Phys. Rev. C **24**, 884 (1981).
[21] Y.-W. Lui, H. L. Clark, and D. H. Youngblood, Phys. Rev. C **64**, 064308 (2001).
[22] B. John, Y. Tokimoto, Y.-W. Lui, H. L. Clark, X. Chen, and D. H. Youngblood, Phys. Rev. C **68**, 014305 (2003).
[23] Y. K. Gupta, U. Garg, J. Matta, D. Patel, T. Peach, J. Hoffman, K. Yoshida, M. Itoh, M. Fujiwara, K. Hara *et al.*, Phys. Lett. B **748**, 343 (2015).
[24] M. Itoh, H. Sakaguchi, M. Uchida, T. Ishikawa, T. Kawabata, T. Murakami, H. Takeda, T. Taki, S. Terashima, N. Tsukahara *et al.*, Phys. Lett. B **549**, 58 (2002).
[25] D. H. Youngblood, Y.-W. Lui, and H. L. Clark, Phys. Rev. C **60**, 014304 (1999).
[26] X. Chen, Y.-W. Lui, H. L. Clark, Y. Tokimoto, and D. H. Youngblood, Phys. Rev. C **80**, 014312 (2009).
[27] D. H. Youngblood, Y.-W. Lui, X. F. Chen, and H. L. Clark, Phys. Rev. C **80**, 064318 (2009).
[28] T. Kawabata, T. Adachi, M. Fujiwara, K. Hatanaka, Y. Ishiguro, M. Itoh, Y. Maeda, H. Matsubara, H. Miyasako, Y. Nozawa *et al.*, Phys. Conf. Ser. **436**, 012009 (2013).
[29] M. Fujiwara, H. Akimune, I. Daito, H. Fujimura, Y. Fujita, K. Hatanaka, H. Ikegami, I. Katayama, K. Nagayama, N. Matsuoka *et al.*, Nucl. Instrum. Methods Phys. Res. A **422**, 484 (1999).
[30] M. Uchida, H. Sakaguchi, M. Itoh, M. Yosoi, T. Kawabata, H. Takeda, Y. Yasuda, T. Murakami, T. Ishikawa, T. Taki *et al.*, Phys. Lett. B **557**, 12 (2003).
[31] G. R. Satchler and D. T. Khoa, Phys. Rev. C **55**, 285 (1997).
[32] T. Li, U. Garg, Y. Liu, R. Marks, B. K. Nayak, P. V. Madhusudhana Rao, M. Fujiwara, H. Hashimoto, K. Nakanishi, S. Okumura *et al.*, Phys. Rev. C **81**, 034309 (2010).
[33] M. Rhoades-Brown, M. H. Macfarlane, and S. C. Pieper, Phys. Rev. C **21**, 2417 (1980).
[34] M. Rhoades-Brown, M. H. Macfarlane, and S. C. Pieper, Phys. Rev. C **21**, 2436 (1980).
[35] S. Raman, C. W. Nestor, Jr., and P. Tikkanen, At. Data and Nucl. Data Tables **78**, 1 (2001).
[36] G. R. Satchler, Nucl. Phys. A **472**, 215 (1987).

[37] M. N. Harakeh and A. E. L. Dieperink, Phys. Rev. C **23**, 2329 (1981).
[38] G. Fricke, C. Bernhardt, K. Heilig, L. A. Schaller, L. Schellenberg, E. B. Shera, and C. W. De Jager, At. Data and Nucl. Data Tables **60**, 177 (1995).
[39] L. D. Rickerston (unpublished).
[40] J. Bartel, P. Quentin, M. Brack, C. Guet, and H. B. Håkansson, Nucl. Phys. A **386**, 79 (1982).
[41] K. Yoshida and N. V. Giai, Phys. Rev. C **78**, 064316 (2008).
[42] B. K. Nayak, U. Garg, M. Hedden, M. Koss, T. Li, Y. Liu, P. V. Madhusudhana Rao, S. Zhu, M. Itoh, H. Sakaguchi *et al.*, Phys. Lett. B **637**, 43 (2006).